Published in final edited form as:
Sci Signal. ; 6(297): ra92. doi:10.1126/scisignal.2004400.

Distinct temporal pattern of T cell receptor signals during positive versus negative selection in situ

Heather J. Melichar[1,*], **Jenny O. Ross**[1,*], **Paul Herzmark**[1], **Kristin A. Hogquist**[2], and **Ellen A. Robey**[1,†]

[1]Division of Immunology and Pathogenesis, Department of Molecular and Cell Biology, University of California, Berkeley, CA 94720, USA

[2]Center for Immunology, University of Minnesota, Minneapolis, MN 55414, USA

Abstract

The recognition by the T cell receptor (TCR) of self peptides presented by the major histocompatibility complex (MHC) controls T cell fate in the thymus, with weak signals inducing survival (the process of positive selection) and stronger signals inducing death (negative selection). In vitro studies have indicated that ligands that give rise to positive selection induce a low, but sustained, pattern of TCR signaling; however, the temporal pattern of TCR signaling in thymocytes that are presented peptide by MHC class I (MHC class I restriction) in they thymus, under conditions that support positive selection, are unknown. Here, we addressed this question by examining intracellular calcium (Ca^{2+}) dynamics and migratory changes in thymocytes undergoing positive and negative selection in thymic slices. We found that brief, serial signaling events that were separated by migratory periods and low cytosolic Ca^{2+} correlated with the positive selection of MHC class I–restricted thymocytes, whereas sustained signaling and arrest of thymocytes were associated with negative selection. Low avidity peptides and the presentation of peptides by cortical thymic epithelial cells failed to induce strong migratory arrest of thymocytes,

†Corresponding author. erobey@berkeley.edu.
*These authors contributed equally to this work.

SUPPLEMENTARY MATERIALS

Fig. S1. Phenotypic comparison of bone marrow–derived and thymic DCs.
Fig. S2. Costimulatory molecules do not significantly contribute to sustained Ca^{2+} signaling during negative selection.
Table S1. Calculation of the frequencies and durations of Ca^{2+} signaling events on the basis of signaling events with defined beginnings and endings
Table S2. Estimates of the duration of Ca^{2+} signaling events based on decay curves.
Movie 1. Signaling patterns of cells undergoing positive and negative selection.
Movie 2. Representative signaling patterns and behavior of cells undergoing positive and negative selection.
Movie 3. Positive selection is associated with brief, serial TCR signaling events.
Movie 4. Thymocytes preferentially arrest in contact with DCs in the presence of agonist peptide.
Movie 5. The stable interactions formed between the thymocyte and DCs in the presence of agonist peptide result in nuclear localization of NFAT.
Movie 6. Thymocytes presented with antigen by cTECs or DCs exhibit distinct signaling and motility patterns.
Movie 7. Representative cell track of the initiation of a signaling event by an OT1tg thymocyte in the presence of OVA peptide presented by DCs.
Movie 8. Increases in ligand potency correlate with a switch from transient to stable interactions of pre-selection OT1tg thymocytes with peptide-loaded DCs.

Author contributions: HM and ER conceived of experiments, HM and JR performed experiments, HM, JR, and ER analyzed data, PH wrote data analysis programs and provided technical assistance, KH provided scientific expertise and reagents, HM, JR, and ER wrote the paper..

Competing interests: The authors declare no competing interests.

which led to transient TCR signaling. Thus, we provide a comparison of positive and negative selection signals in situ and suggest that the absence of strong stop signals is an important feature that distinguishes between positive and negative selection.

INTRODUCTION

During T cell development, the T cell receptors (TCRs) found on the surface of thymocytes (T cell precursors) are screened for their ability to recognize peptide-bound major histocompatibility complexes (pMHCs) when the thymocytes are at the immature $CD4^+CD8^+$ (double positive, DP) stage, a process known as positive selection. Additionally, auto-reactive DP thymocytes, as well as $CD4^+$ and $CD8^+$ single positive (SP) thymocytes, are eliminated during a process known as negative selection to produce a protective, yet self-tolerant, repertoire of T cells. One widely held model of thymocyte selection posits that weak TCR signals promote thymocyte survival and differentiation, whereas stronger signals lead to deletion of the cells by negative selection (1). It is unclear, however, how this difference in signal strength relates to the duration and frequency of TCR signaling events and the dynamics of contact between thymocytes and pMHC-bearing cells. Moreover, positive and negative selection are mediated by distinct cell types within the thymus, but the contribution of the type of peptide-presenting cell to the temporal pattern of TCR signaling during positive versus negative selection is not known.

In a landmark study that sought to identify differences in signaling during positive and negative selection, thymocytes were stimulated in vitro using soluble TCR ligands in the form of tetramerized peptide-MHC complexes (MHC-tetramers) (2). The authors observed low, sustained increases in cytosolic Ca^{2+} concentration in response to low-affinity peptides and strong, transient increases in Ca^{2+} concentration in response to high-affinity peptides. In addition, this group also identified a sharp affinity threshold that correlated with these signaling differences and with the ability of these peptides to induce positive versus negative selection in fetal thymic organ culture (FTOC) (2). Although this study provided key information about the role of peptide affinity in determining the distinct signals representative of positive and negative selection, it did not allow for the dissection of other critical factors that contribute to thymocyte selection in vivo, including the nature of the pMHC-bearing cells and the effect of thymocyte motility. This information is crucial given that thymocytes only undergo efficient positive selection when in contact with a three-dimensional (3D) stromal cell network, as well as the observation that immature thymocytes are highly motile within this network (3–9).

Dynamic imaging of thymocytes within thymic tissue slices has revealed that TCR-induced Ca^{2+} signals associated with positive selection induce migratory arrest (9). This finding suggests that the Ca^{2+} flux generated upon the initial encounter with positive selecting ligands helps to prolong the interaction with pMHC-bearing stromal cells, which is estimated to last for 15 to 30 min in this system (9). This study examined MHC class II–restricted positive selection, and there are indications that the signals for the positive selection of MHC class I–restricted thymocytes are weaker or of shorter duration (10, 11). Moreover, this study focused on positive selection; thus, how the kinetics of TCR signaling

and thymocyte migration differ during positive and negative selection has not yet been examined.

Here, we used changes in cytosolic Ca^{2+} concentrations and cell motility to monitor MHC class I–restricted TCR signaling events in thymocytes undergoing positive or negative selection in thymic slices (in situ). We observed that in contrast to the sustained signals observed after stimulation of MHC class I–restricted thymocytes with low-potency peptides in vitro, thymocytes in our system underwent brief (~4 min) and relatively infrequent (~1 to 2 per hour) signaling events that were separated by periods of migration and low cytosolic Ca^{2+} concentrations during positive selection in situ. During negative selection, however, more thymocytes experienced prolonged signaling events that were characterized by persistently enhanced intracellular Ca^{2+} concentrations, translocation of the transcription factor NFAT (nuclear factor of activated T cells) to the nucleus, and migratory arrest. We tested the role of ligand potency and the type of pMHC-bearing cell and found that lower potency peptides and presentation by radiation-resistant thymic stromal cells contributed to the more transient signaling events that were associated with positive selection. These findings provide a direct comparison of the temporal pattern of TCR signaling and motility changes during positive and negative selection within living thymic tissue, and they suggest that the absence of strong stop signals and transient TCR signaling events are important features that distinguish positive from negative selection.

RESULTS

Synchronized positive and negative selection occurs in thymic slices

To establish the ability of the thymic slice model to support the positive selection of MHC class I–restricted thymocytes, we used a relatively homogeneous population of pre-selection TCR transgenic (tg) DP thymocytes overlaid on thymic slices in the presence or absence of a positively selecting peptide ligand. Pre-selection OT1 TCR transgenic, *Rag2*-deficient DP thymocytes (herein called OT1tg cells) were overlaid onto thymic slices from $H2^b$ mice (hereafter referred to as wild-type slices), which provide a positive-selecting environment, or from MHC-deficient (knockout) mice (MHCko), which provide a non-selecting environment, and we assessed the differentiation of the OT1tg DP cells into $CD8^+$ SP thymocytes over time by flow cytometry. OT1tg cells on wild-type thymic slices gave rise to a substantial population of $CD8^+$ SP cells at 72 hours (Fig. 1, A and B). In contrast, OT1tg thymocytes on MHCko slices failed to exhibit an increase in the cell-surface abundance of CD69, a marker of cellular activation, and they maintained the presence of both CD4 and CD8 over time (Fig. 1, A and B). The $CD8^+$ SP cells that developed on wild-type thymic slices had the conventional CD8αβ heterodimer and exhibited reduced cell-surface abundance of CD24, which suggested that they had developed into mature, conventional $CD8^+$ SP cells (Fig. 1, C and D). In addition, $CD8^+$ SP cells generated in thymic slices were functionally mature, as indicated by their increased production of granzyme B and interferon-γ (IFN-γ) after they were stimulated through the TCR with anti-CD3 and anti-CD28 antibodies in vitro (Fig. 1E). Addition of the negatively selecting ovalbumin (OVA) peptide to the wild-type thymic slice induced a more marked increase in CD69 abundance on the OT1tg thymocytes than occurred on wild-type slices alone, which was followed by a

substantial depletion in the numbers of OT1tg DP cells after 24 hours (Fig. 1A). We obtained similar results in experiments with another MHC class I–restricted system, the HY^{CD4} TCR transgenic mouse, which models negative selection to endogenous male antigen (12). Mature, T3.70$^+$ (HY TCR$^+$) CD8$^+$ SP thymocytes emerged in slices prepared from female wild-type mice (providing evidence of positive selection), whereas a reduction in the number of DP thymocytes without an accompanying increase in the number of CD8$^+$ SP cells occurred on slices from male WT mice (which is indicative of negative selection) (Fig. 1F). These data demonstrate the ability of this experimental model to support a synchronized wave of pre-selection MHC class I–restricted DP thymocytes undergoing positive and negative selection in situ.

Distinct TCR signaling and migratory properties distinguish between positive and negative selection in situ

Much of our information about the TCR signaling events that influence thymic selection derives from studies of dissociated thymocytes under in vitro conditions that do not support positive selection and in which thymocytes are non-motile. To directly examine TCR signals and thymocyte motility during positive selection through MHC class I, we loaded OT1tg cells with a ratiometric calcium indicator dye, Indo-1 LR, and overlaid the thymocytes onto thymic slices taken from either wild-type or MHCko mice. We then imaged the labeled OT1tg thymocytes within the slices by two-photon time-lapse microscopy within 2 to 4 hours of the addition of the thymocytes to the slices. Pre-selection DP thymocytes actively migrate and localize preferentially to cortical regions of thymic slices (4, 5, 9), which enabled us to track individual thymocytes in the cortex over time and determine the ratio of the fluorescent signal of Ca^{2+}-bound to unbound Indo-1 for each thymocyte at each time point. We expressed the ratio of the fluorescent signals of bound and unbound dye (the Ca^{2+} ratio) as a corrected value by subtracting the average Ca^{2+} ratio of thymocytes on non-selecting slices from all other experimental conditions, and we displayed the distribution of Ca^{2+} values for each thymocyte at each time point (Fig. 2, A and B, and movie S1). We noted a modest, but reproducible, increase in the frequency of time points in which OT1tg DP thymocytes showed elevated cytosolic Ca^{2+} (with a corrected Ca^{2+} ratio >0.15) in wild-type compared to MHCko slices, consistent with the relatively low-intensity signals predicted for positive selection.

If the increase in the frequency of time points in which thymocytes on wild-type slices had elevated cytosolic Ca^{2+} compared to thymocytes on MHCko slices was a result of positive selection, we would expect it to depend on MHC class I found on thymic epithelial cells. To test this, we restricted MHC class I to irradiation resistant thymic stromal cells using thymic slices from radiation bone marrow chimeric mice in which MHCko hematopoietic cells developed in irradiated WT hosts (referred to as MHCko→wild-type slices). Previous studies have reported increased numbers of positively selected polyclonal thymocytes in MHCko→wild-type chimeras, which is indicative of positive selection that is relatively unopposed by negative selection (13–15). When we introduced pre-selection OT1tg thymocytes onto thymic slices from MHCko→wild-type bone marrow chimeric mice, we again observed a modest increase in the frequency of cells that exhibited increased Ca^{2+} signaling compared to those on MHCko slices, a change that was comparable to that

observed when OT1tg thymocytes were introduced onto wild-type slices (Fig. 2, A and B). In contrast, OT1tg thymocytes on wild-type slices to which the negatively selecting OVA peptide was added (wild-type + OVA) displayed a substantial increase in the frequency of time points with increased cytosolic Ca^{2+} concentrations (Fig. 2, A and B, and movie S1), consistent with the more intense TCR signals predicted for negative selection. We observed a similar trend for HY^{CD4}tg thymocytes, in which thymocytes on thymic slices from male mice (a negative-selecting environment) displayed more Ca^{2+} signals compared to thymocytes placed on slices from WT female mice (a positive-selecting environment) (Fig. 2, C and D). Note that the frequency and magnitude of the changes in Ca^{2+} concentrations in HY^{CD4}tg thymocytes were reduced compared to those in OT1tg thymocytes (Fig. 2, A to D), which may have been because only ~50% of DP thymocytes are $TCRtg^{+}$ in this model (12), or because of the lower affinity or abundance of the negative-selecting peptide.

An examination of cytosolic Ca^{2+} signals in individual thymocytes revealed distinct temporal patterns of changes in Ca^{2+} concentration that predominated under positive-selecting rather than negative-selecting conditions (Fig. 2, E to G, and movie S2). Whereas many OT1 and HY^{CD4}tg thymocytes in negative-selecting slices showed consistently increased Ca^{2+} concentrations over the entire track (with average corrected Ca^{2+} ratios for the track of >0.1, with at least one time point with a ratio >0.2, designated “hi”), most signaling thymocytes under positive-selecting conditions displayed transient increases in Ca^{2+} concentration, with the remainder of the track displaying Ca^{2+} concentrations near background (with an average corrected Ca^{2+} ratio of track <0.1, with at least one time point with a ratio >0.2, designated “lo-hi”). We did not observe prominent thymocyte death under negative-selecting conditions, consistent with previous evidence of a 4- to 12-hour lag between the initial encounter with negative selecting ligands and thymocyte death (16). Together, these data suggest that positive selection of MHC class I–restricted thymocytes is associated with transient increases in cytosolic Ca^{2+} concentration, whereas negative selection is associated with more sustained signals.

To explore the relationship between changes in Ca^{2+} concentration and cell migration in our system, we categorized thymocyte tracks into lo, lo-hi, and hi categories, and plotted their average speeds and directionality for the different selection conditions (Fig. 3A). This analysis revealed that thymocytes with low Ca^{2+} concentrations, which were most prominent in non-selecting, MHCko slices, displayed the greater speeds and straighter tracks. In contrast, thymocytes displaying sustained increases in Ca^{2+} concentrations, which predominated under negative selecting (wild-type+OVA) conditions, tended to be slower and had more confined areas of movement (Fig. 3, A to C, and movie S2). Moreover, for thymocytes in the lo-hi category, which predominated in positive-selecting (wild-type) slices, an inverse relationship between Ca^{2+} concentration and migration speed was observed as brief migratory pauses that coincided with transient increases in cytosolic Ca^{2+} concentrations (Fig. 3B and movie S2), consistent with previous reports (9, 17–19). The predominance of thymocytes with sustained Ca^{2+} signaling and low motility in negative-selecting (wild-type+OVA) conditions was unlikely to be an artifact of the use of supraphysiological concentrations of agonist (negatively selecting) OVA peptide, because similar responses were observed in experiments with HY^{CD4}tg thymocytes in response to endogenous, negative-selecting signals (Fig. 2G). Moreover, in a study of the negative

selection of thymocytes, very low concentrations of agonist peptide induced all-or-nothing Ca^{2+} signaling and migratory arrest (16). Thus, a range of negative-selecting conditions led to migratory arrest and sustained Ca^{2+} signaling, whereas positive-selecting conditions were associated with brief, transient Ca^{2+} signals and continued migration.

Migratory pauses that occurred with brief increases in cytosolic Ca^{2+} concentration likely corresponded to transient periods of active TCR signaling during which thymocytes were engaged by positive-selecting ligands. In addition, it is unlikely that thymocytes engaged positive-selecting ligands on immobile thymic epithelial cells while rapidly migrating and displaying low intracellular Ca^{2+} abundance. We therefore used both motility and Ca^{2+} abundance to define the beginning and end of transient "signaling events" in thymocytes under conditions of positive selection (Fig. 3B, lower panel, and table S1). We initially identified signaling events as portions of the cell track during which thymocytes displayed corrected Ca^{2+} ratios >0.2. We then defined "non-signaling" portions of the track as time points in which the interval speed was >6 microns/min and the corrected Ca^{2+} ratio was <0.1 (Fig. 3B, lower panel). We considered a signaling event to have a beginning when a non-signaling portion of the track preceded it, and to have an end when a non-signaling portion of the track followed it. Based on these criteria, we estimated that the average duration of transient signaling events for OT1tg thymocytes on positive selecting slices (either wild-type or MHC→wild-type slices) was ~4 min (Fig. 3D and Table S1). We note that these calculations did not include signaling events that were bounded by the beginning or end of the imaging run, or were a result of a cell leaving the imaging volume. We also collated the full range of durations, including those without defined beginning and ends (Fig. 3F).

We also estimated the frequency of signaling events to be the total number of signaling events that began during the run divided by the cumulative track imaging time (table S1). The number of observed signaling events during the cumulative imaging hours suggested a frequency of 1 signaling event every 31 min or 1 event every 36 min for OT1tg thymocytes on slices from wild-type mice or MHCko→WT chimeric mice, respectively (Fig. 3E and table S1). The duration of the imaging runs was typically 20 min, and thus most of the tracks contained one or no signaling events. However, we did occasionally observe tracks that had two signaling events that were separated by a period of migration and low changes in cytosolic Ca^{2+} concentration (movie S3). Under non-selecting conditions (in MHCko slices), thymocytes also displayed occasional calcium "events," although these were of substantially shorter duration and reduced frequency than those of thymocyes under positive selecting conditions. Together, these data suggest that brief, serial signaling events underlie the process of positive selection.

Thymocytes arrest and signal adjacent to cortical DCs during negative selection

In contrast to the transient signals associated with positive selection, the prolonged migratory arrest of thymocytes in the presence of agonist (negatively selecting) peptide suggested that they had relatively monogamous interactions with pMHC-bearing cells. Although any MHC class I–expressing cell in the thymus could potentially present OVA peptide in our system, we considered whether thymic dendritic cells (DCs) might play a predominant role in inducing negative selection. Thymic DCs have been implicated in

negative selection and, although thymic DCs are most prominent in the medulla, there is also an extensive DC network in the cortex that enables frequent encounters between thymocytes and DCs to occur (6, 20). To test whether cortical thymic DCs preferentially presented negative-selecting ligands to thymocytes, we overlaid pre-selection OT1tg DP thymocytes onto thymic slices from mice expressing a fluorescent DC reporter, CD11c fused to yellow fluorescent protein (CD11c-YFP) (21). Time-lapse imaging revealed that the CD11c-YFP–labeled thymic DCs were non-motile, but that they displayed probing and retraction movements of dendrites, consistent with previous observations (movie S4) (6). In the absence of OVA peptide, thymocytes migrated in the vicinity of DCs, but they did not form stable contacts, maintaining an average distance of ~5 microns from the nearest DC (Fig. 4, A and B, and movie S4). The addition of OVA peptide to the thymic slices led to the arrest of thymocytes adjacent to DCs, which resulted in a reduction in the average distance from the thymocyte to the nearest DC, particularly for those thymocytes with the lowest speeds (Fig. 4, A and B, and movie S4).

To confirm that the thymocytes that arrested near to cortical DCs received negative selection signals, we used a nuclear factor of activated T cells (NFAT)—green fluorescent protein (NFAT-GFP) fusion protein to monitor TCR signaling. The transcription factor NFAT translocates from the cytosol to the nucleus in response to TCR signaling, and an NFAT-GFP fusion protein was previously used to monitor TCR signaling by time-lapse microscopy both in vitro and in vivo (22–25). In addition, we also took advantage of the inherent autofluorescence of thymic DCs to simultaneously monitor thymocyte-DC contacts and the subcellular localization of NFAT in thymocytes. The morphology and distribution of autofluorescent cells in wild-type thymic slices was similar to that of cells expressing the CD11c-YFP DC reporter (Fig. 4C, top panels), consistent with their identification as DCs. Two-photon microscopic analysis of thymocytes in positive selecting slices revealed freely migrating thymocytes displaying an accumulation of NFAT-GFP at the cell periphery, consistent with the cytosolic location of the fusion protein (Fig. 4C, middle panels, and movie S5). The addition of OVA peptide led to the appearance of a population of thymocytes displaying a more central accumulation of NFAT-GFP, consistent with its nuclear localization (Fig. 4C, bottom panels, cell #1, and movie S5). Thymocytes with central NFAT accumulation were typically arrested near autofluorescent cells with dendritic morphology, whereas the more motile thymocytes in the same imaging volume displayed a more peripheral accumulation of NFAT (Fig. 4C, bottom panels, cell #2, and movie S5). To quantify the relative abundances of nuclear and cytosolic NFAT-GFP in thymocytes, we determined the volume of the cell based on a relatively high threshold of NFAT-GFP fluorescence intensity, such that thymocytes with centralized accumulation of NFAT-GFP appeared to occupy smaller volumes compared to those of thymocytes that exhibited a peripheral accumulation of NFAT-GFP (Fig. 4D). This trend was most obvious for the slowest moving cells (Fig. 4E). Thus, in response to a broadly distributed agonist peptide, thymocytes preferentially arrested and signal while in contact with cortical DCs.

Presentation of agonist peptide by cortical thymic epithelial cells or DCs leads to distinct thymocyte responses

The localization of thymocytes in close proximity to OVA-bearing DCs suggests that thymocytes preferentially arrest in response to agonist peptide presented by DCs. This is despite the presence of OVA peptide on other MHC class I–bearing cells, including thymic epithelial cells (TECs). To determine the relative contributions of pMHC presentation by cortical TECs (cTECs) and DCs to thymocyte signaling and migratory arrest, we modified our experimental system to limit MHC class I to particular cell types. To restrict OVA peptide presentation to thymic stromal cells (including cTECs), we prepared thymic slices from MHCko→wild-type bone marrow chimeric mice and added OT1tg thymocytes and, subsequently, OVA peptide to the slices (stroma+OVA). Conversely, to restrict OVA presentation to DCs, we added bone marrow–derived DCs that had been pre-loaded with OVA peptide to MHCko thymic slices containing pre-selection OT1tg DP thymocytes (DC +OVA). We then assessed thymocyte activation and deletion by flow cytometry, whereas we used two-photon microscopy to monitor cell motility and cytosolic Ca^{2+} signaling. Although bone marrow–derived DCs are phenotypically distinct from thymic DCs (fig. S1), a subset were able to enter the thymic slices and induce efficient negative selection of thymocytes in situ (Fig. 5A), suggesting that they provide a reasonable surrogate for endogenous thymic DCs.

The presence of OVA peptide, whether presented by stromal cells or DCs, correlated with a substantial increase in the cell-surface abundance of CD69 and a loss of DP thymocytes compared to positive-selecting or non-selecting conditions (Fig. 5, A and B). However, restriction of OVA peptide presentation to the stromal cell compartment reduced the extent of negative selection compared to that in samples in which OVA peptide presentation was restricted to DCs, as indicated by the less substantial increase in CD69 abundance and the reduced depletion of DP thymocytes (Fig. 5, A and B). This decrease in the efficiency of negative selection correlated with reduced TCR signals, with thymocytes from slices in which stromal cells presented OVA displaying a decreased frequency of time points in which cytosolic Ca^{2+} signaling was increased (Fig. 5, C and D), as well as a reduced percentage of tracks in the “hi” (sustained signaling) category (Fig. 5E).

Increases in cytosolic Ca^{2+} concentration can lead to migratory arrest, thus prolonging interactions with pMHC-bearing cells and promoting sustained signals (9, 18). To examine the influence of the type of APC on migratory arrest, we compared the motility of thymocytes under conditions in which either DCs or thymic stromal cells presented OVA peptide (Fig. 5F). In the presence of OVA peptide presented by DCs, thymocytes with persistently increased Ca^{2+} signaling (“hi” category) showed low motility, consistent with strong migratory arrest (Fig. 5F). However, when OVA peptide presentation was restricted to the thymic stromal cells, a substantial proportion of thymocytes in the “hi” signaling category remained motile or regained motility, indicating a diminished “stop” signal (Fig. 5F and movie S6).

To further compare the Ca^{2+}-induced stop signal provided by DCs with that provided by stromal cells, we defined a “typical” signaling event under different experimental conditions. To do so, we identified multiple cell tracks that contained signaling events that

began during the imaging run based on a period of increased Ca^{2+} concentration (that is, a corrected Ca^{2+} ratio >0.2) preceded by a non-signaling period (cell speed >6 microns/min and a corrected Ca^{2+} ratio of <0.1). We then aligned these tracks based on the first signaling time point in each track, and we calculated the average Ca^{2+} ratios and speeds for all of the tracks relative to the onset of the signaling event (Fig. 5G). OT1tg thymocytes on a positive-selecting slice (MHCko→wild-type chimeras) displayed a rapid drop in motility coincident with the initial rise in cytosolic Ca^{2+} concentration, and returned to rapid motility and baseline Ca^{2+} concentrations after several minutes (Fig. 5G). For thymocytes in the presence of OVA peptide–loaded DCs, most signaling thymocytes in these samples had low motility and persistently increased Ca^{2+} concentrations, suggesting that they were already actively signaling at the beginning of the analysis (Fig. 5, E and F). However, approximately 12% (14 out of 118 tracks) displayed high motility and low Ca^{2+} signaling at the beginning of the analysis and then underwent rapid arrest with increased cytosolic Ca^{2+} concentrations, indicative of the beginning of a signaling event (Fig. 5G and movie S7). Alignment and averaging of these events revealed that Ca^{2+} concentrations in response to negative selection signals (DC+OVA) remained well above background, and thymocytes remained arrested for the duration of the imaging run (Fig. 5G). Thymocytes in the presence of OVAp presented by radiation-resistant stromal cells displayed an intermediate behavior, with a detectable, but reduced stop signal (Fig. 5G). These analyses confirmed that thymic stromal cells were less effective than DCs at inducing persistent TCR signaling and migratory arrest.

We then used decay analysis to examine the relative stabilities of TCR signaling events in thymocytes that were engaged by OVA peptide on DCs compared to those in thymocytes engaged by OVA peptide on cTECs (Fig. 5H and table S2). For thymocytes that were signaling at the beginning of each imaging run, we determined when the signaling event ended based on both a reduction in Ca^{2+} concentration (having a Ca^{2+} ratio of <0.1) and an increase in motility (having an interval speed >6 microns/min). We then determined the proportion of thymocytes that continued signaling over the 20-min imaging run under different conditions (Fig. 5H and table S2). For the positive-selecting environments of wild-type slices and MHCko→wild-type slices, approximately half of the signaling events terminated ~6 min into the run, and fitting the data to a first-order decay equation yielded mean lifetimes of 9 and 11 min, respectively (table S2). These lifetimes are in reasonable agreement with our estimates (albeit slightly higher) of the duration of signaling events based on events with beginnings and ends (table S1), In contrast, thymocytes in the presence of OVA peptide–loaded DCs exhibited stable signaling events, with 68% lasting longer than the imaging run (>20 min), corresponding to a mean lifetime of 58 min (table S2). Thymocytes on thymic slices in which stromal cells presented OVA showed slightly reduced stability of signaling events relative to those on slices in which DCs presented OVA, with 52% of signaling events persisting beyond 20 min, corresponding to a mean lifetime of 34 min. These data further suggest that an encounter with a negative-selecting peptide presented by thymic stromal cells provided a weaker stop signal than did an encounter with the same peptide presented by DCs.

One important feature of DCs that may contribute to their ability to promote migratory arrest and sustained signaling is their expression of co-stimulatory and adhesion molecules, such as intercellular adhesion molecule 1 ICAM-1. To examine the contribution of co-stimulatory

molecules, we isolated DCs from ICAM-1–deficient mice (26, 27) and tested their ability to cause migratory arrest and TCR signaling when they presented OVA peptide to pre-selection OT1tg DP thymocytes on MHCko thymic slices. We observed a modest, but reproducible, reduction in the frequency of time points in which thymocytes had increased Ca^{2+} signaling when incubated with ICAM-1–deficient DCs compared to when they were incubated with wild-type DCs (Fig. 6, A and B). In addition, in the presence of ICAM-deficient DCs we observed a reduced percentage of thymocytes that exhibited consistently increased Ca^{2+} signaling, with some of the cells that exhibited tracks with increased Ca^{2+} signaling remaining motile or regaining motility (Fig. 6, C and D).

We obtained similar results from experiments with DCs from mice doubly deficient in the costimulatory molecules B7.1 and B7.2, although there was considerable variability in the data, and the difference between the effects of these DCs and those of wild-type DCs did not reach statistical significance (fig. S2). In contrast to the 68% of signaling events that persisted beyond 20 min when wild-type DCs presented OVA peptide, only 40% of signaling events persisted beyond 20 min when OVA peptide was presented by ICAM-1–deficient DCs, (Fig. 6E). These differences in the extent and duration of Ca^{2+} signals between wild-type and the various mutant DCs correlated with a reduced increase in CD69 abundance (Fig. 6F), although ICAM-1–deficient DCs induced negative selection to a degree similar to that of wild-type DCs (Fig. 6G). These data suggest that ICAM-1 plays a contributing, but nonessential, role in promoting sustained Ca^{2+} signals during negative selection, and that, in the absence of ICAM-1 or B7 molecules, other factors are sufficient to enable relatively efficient negative selection to occur in this system.

Only high-potency ligands efficiently induce migratory arrest and sustained TCR signals

The strength of binding of the TCR to pMHC is thought to be an important parameter in distinguishing between positive and negative selection. To investigate the role of ligand potency on TCR signaling in situ, we used a panel of altered peptide ligands (APLs) that were previously characterized for their relative potencies and abilities to induce the positive or negative selection of OT1tg thymocytes in FTOC. The relative potency of the peptides to stimulate T cells was OVAp > Q4 > T4 > Q7, with OVAp and Q4 inducing negative selection, Q7 supporting positive selection, and T4 at the threshold between positive and negative selection (2). We overlaid pre-selection OT1tg DP cells onto MHCko thymic slices, added DCs loaded with peptides of different affinities, and examined cellular activation and deletion by flow cytometric analysis, as well as monitored changes in cytosolic Ca^{2+} concentration and motility by time-lapse two-photon microscopy. OVA peptide variants induced a gradient of responses in terms of the increase in cell-surface CD69 abundance and the deletion of DP thymocytes, correlating with their previously described potency (2) (Fig. 7, A and B). Ligand potency also correlated with an increase in the proportion of time points displaying increased cytosolic Ca^{2+} concentrations, and an increase in the proportion of thymocytes that exhibited persistently enhanced Ca^{2+} signaling (Fig. 7, C and D). Moreover, DCs loaded with higher potency peptides exhibited more stable interactions with thymocytes (Fig. 7E and movie S8). For peptides at or below the previously defined threshold between positive and negative selection (T4 and Q7), some thymocytes with enhanced Ca^{2+} signaling remained motile, whereas for peptides with

potencies above the threshold leading to negative selection (Q4 and OVA), almost all of the thymocytes with enhanced Ca^{2+} concentrations displayed low motility (Fig. 7F). In addition, whereas for the Q4 and OVA peptides, 58% (Q4) and 68% (OVA) of thymocytes that were signaling at the beginning of the run remained signaling for >20 min, only 40 and 42% were still signaling after 20 min in the presence of the T4 and Q7 peptides, respectively (Fig. 7G). Thus, only high potency peptides induced a strong, TCR-mediated stop signal in this system.

DISCUSSION

The magnitude and duration of signaling events determine downstream transcriptional programs and developmental outcomes, yet little is known about the patterns of TCR signaling in thymocytes undergoing positive or negative selection in situ. Here, we used two-photon microscopy to define TCR signaling during MHC class I–restricted thymocyte selection in situ under conditions that preserved the dynamic migration of thymocytes and their diverse cellular encounters within intact thymic tissue. We found that whereas negative selection was associated with prolonged TCR signaling and stable cellular interactions, positive selection involved surprisingly brief and infrequent TCR signals. We also investigated the specific contributions of the type of peptide-presenting cell, costimulatory signals, and ligand potency to the pattern of TCR signaling. We found that each of these factors contributed to generating the distinct TCR signaling and intercellular interactions characteristic of positive and negative selection. Our data shed light on how different components of the thymic microenvironment contribute to temporal TCR signaling patterns during positive and negative selection.

The brief Ca^{2+} signaling events that we observed during positive selection in situ are in sharp contrast to the sustained rise in cytosolic Ca^{2+} concentrations observed when OT1tg thymocytes are stimulated in vitro with MHC class I tetramers loaded with low-potency peptides (2). Although the reason for this difference is not yet clear, it is tempting to speculate that the motility of thymocytes and the dynamics of contacts with pMHC-bearing thymic stromal cells may contribute to the distinct temporal pattern of signaling, and ultimately to the ability of thymocytes to successfully undergo positive selection. We propose that the tendency of thymocytes to migrate away from pMHC-bearing stromal cells may disrupt TCR engagement and thus favor transient signals. We further speculate that transient TCR engagement and dynamic contacts with pMHC-bearing cells may be sufficient to enable the generation of survival signals while avoiding negative selection. This may help to explain the requirement for a 3D stromal cell network for efficient positive selection.

Although positive selection is thought to involve relatively weak TCR signals, there are indications that the positive selection of $CD4^+$ T cells may involve somewhat more intense and long-lasting signals than are required for the positive selection of $CD8^+$ T cells (10, 11). In this context, it is interesting to compare our results from experiments with MHC class I–restricted OT1tg cells with the results of a previous study of Ca^{2+} signals during the positive selection of thymocytes bearing an MHC class II–restricted TCR (9). Although transient signals were also noted in that study, the signals were estimated to last for 15 to 30 min, rather than the ~4 min that we reported here. This difference in the duration of TCR signals

during MHC class I– versus MHC class II–dependent positive selection is consistent with the requirement for factors that prolong Ca^{2+} signals in response to weak TCR ligands for the development of $CD4^+$, but not $CD8^+$, T cells (28). We and others have previously noted that MHC is required to sustain the low-level abundance of activation markers and thymocyte motility in polyclonal DP cells, which is suggestive of low-level tonic TCR signals (5, 6, 29, 30). It is possible that the brief, infrequent signaling events that we reported here correspond to these tonic TCR signals and are sufficient to enable the positive selection of $CD8^+$ T cells.

The correlation of positive selection with continued motility and transient Ca^{2+} signals raises the question of whether negative selection invariably involves migratory arrest and prolonged signaling. In support of this, we observed a close correlation between the prevalence of immobile, persistently signaling thymocytes and the extent of negative selection under various experimental conditions. In addition, a parallel study examining the negative selection of more mature thymocytes showed that very low concentrations of agonist peptide stimulated all-or-nothing responses that were characterized by rapid migratory arrest and prolonged Ca^{2+} signals, consistent with evidence that suggests that agonist peptide can induce negative selection, but is ineffective at inducing positive selection, even at very low concentrations (16, 31). On the other hand, in a previous study of a steady-state model of autoimmune regulator (AIRE) -dependent negative selection to tissue restricted antigen in the medulla, we observed a population of thymocytes that remained motile within confinement zones in the medulla, which implies that not all thymocytes remain permanently immobile after encountering negative-selecting ligands (7). Note that this study examined a steady-state population of thymocytes, and it was unclear when individual thymocytes first encountered negative-selecting ligands. Indeed, we have reported that thymocyte death can occur between 4 and 12 hours after synchronous encounter with a negative-selecting ligand, leaving an extended time window during which thymocytes could potentially integrate death and survival signals (16). Together, these observations suggest a model in which the initial encounter with a negative-selecting ligand leads to migratory arrest and prolonged TCR signaling, but under conditions of suboptimal negative-selection signals, some thymocytes may get a reprieve. These cells may eventually recover their motility and continue to sample the thymic environment while deciding whether to die or undergo an alternate form of thymic selection giving rise to regulatory T cell populations, a phenomenon that has been termed agonist selection (31).

Previous studies of mature T cells showed that T cell interactions with DCs presenting moderate potency ligands, such as the OVA variant, T4, leads to motile signaling contacts termed kinapses (32–34). Consistent with this, we observed a progressive decrease in sustained Ca^{2+} signals and migratory arrest for thymocytes in the presence of DCs loaded with peptides of decreasing affinity for the TCR. APLs with affinities above the previously defined positive-negative selection boundary tended to carry a stronger “stop signal.” However, we did not observe a sharp transition in the temporal pattern of signaling, as was reported for in vitro stimulation with pMHC tetramers (2). It is important to note, though, that neither the stimulation of thymocytes with tetramers nor the presentation of antigens by DCs supports positive selection. For example, in our study, even low-potency, “positively selecting” APLs induced some negative selection. Additional studies will be needed to fully

address the question of how peptide affinity and the type of peptide-presenting cell combine to enable appropriate T cell development.

Whereas much negative selection occurs in the thymic medulla after positive selection, there is increasing evidence that negative selection to ubiquitous self-antigens can occur in the thymic cortex, and that a large proportion of DP thymocytes is deleted as a result of negative selection (12, 20, 35, 36). Given the unique ability of cTECs to mediate positive selection, it is of interest to determine how thymocytes would respond if they encountered high-potency ligands on cTECs. Here, we presented two lines of evidence that suggest that the presentation of high-potency ligands displayed by cTECs are much less efficient at inducing stop signals than the same ligands presented by DCs. First, thymocytes preferentially arrested and exhibited prolonged Ca^{2+} signaling when adjacent to cortical DCs, despite the fact that soluble agonist peptide was added to the slice and was presumably presented by all MHC class I–bearing cells, including cTECs. In addition, thymic slices in which MHC class I was restricted to radiation-resistant thymic stromal cells (including cTECs) did not support prolonged migratory arrest and sustained Ca^{2+} signaling in response to strong agonist peptide, which correlated with inefficient negative selection.

In summary, in our study we compared the temporal patterns of TCR signaling during the positive and negative selection of thymocytes in situ, and revealed the distinct ability of cTECs to provide TCR-mediated signals to developing thymocytes without inducing prolonged Ca^{2+} signals and strong migratory arrest. cTECs have a number of other properties that likely contribute to their ability to induce positive selection. These include specialized machinery to generate distinct endogenous peptides, and a relative lack of co-stimulatory molecules (37–40). Future studies combining genetic manipulation of cTECs together with imaging of thymocyte signaling and migration in situ should help to address the question of how these properties of cTECs enable them to deliver survival signals to thymocytes while avoiding negative selection.

MATERIALS AND METHODS

Mice and bone marrow chimeras

All mice were maintained at the American Association of Laboratory Animal Care–approved facility in the Life Sciences Addition at the University of California, Berkeley, CA under pathogen-free conditions. All animal procedures were approved by the Animal Care and Use Committee. CD11cYFP transgenic and Act-CFP transgenic mice were bred in-house (21, 41). Pre-selection OT1tg Rag2KO Ly5.1 or OT1tg Rag2KO Ubi-GFP tg thymocytes were generated by transferring 1 to 5×10^6 bone marrow cells intravenously into lethally irradiated, non-selecting 3- to 6-week old MHC I–deficient ($B2m^{-/-}$, Taconic) or MHC I and MHC II double knockout mice (MHCko, Abb-B2m, Taconic) and were allowed to reconstitute for 5 to 12 weeks before being used for experiments (42–44). Chimeras that were used for experiments had a minimum of 70% OT1tg DP cells. Alternatively, OT1tg Rag2KO mice were crossed onto a MHC I (B2m)-deficient background. Pre-selection HY^{CD4}tg thymocytes were maintained on a non-selecting H2-Db–deficient background (20). Pre-selection HY^{CD4}tg cells were depleted of cells expressing endogenous TCRs by negative enrichment with the EasySep Biotin Positive

Selection Kit (STEMCELL Technologies) as directed by the manufacturer with biotin-conjugated anti-CD69 antibody (eBioscience). Cells that were used for experiments had a minimum of 55% T3.70^{+} HY^{CD4}tg DP cells. To generate chimeras with radiation-resistant stromal cell–restricted MHC expression, wild-type (WT) C57BL/6 mice were administered purified anti-NK1.1 antibody (UCSF Monoclonal Antibody Core) by intraperitoneal injection and then were irradiated with two doses of 600 rads before receiving an intravenous injection of bone marrow from MHCko mice. To generate NFAT-GFP–expressing pre-selection OTI tg cells, OT1 tg mice were injected with 5-fluorouracil (Sigma), and bone marrow harvested from the mice was cultured in Dulbecco's Modified Eagle Medium (DMEM) containing 10% fetal bovine serum, pencillin/streptomycin and recombinant mouse interleukin-3 (rmIL-3, 20 ng/ml), rmIL-6 (50 ng/ml), and recombinant mouse stem cell factor (rmSCF, 50 ng/ml). All cytokines were obtained from Peprotech. Phoenix E cells were transfected with retroviral vector encoding NFAT-GFP with Lipofectamine Plus reagent according to the manufacturer's protocol. Cell culture medium containing virus particles was mixed with polybrene (4 μg/ml) and was used to spin-infect bone marrow cells. Non-selecting recipient mice were irradiated with two doses of 600 rads and then were intravenously injected with 0.5 to 5 × 10^6 transduced cells.

Thymic slices

Vibratome-cut thymic slices were prepared essentially as described previously (45). Individual thymic lobes were embedded in 4% low-melt agarose dissolved in Hank's Balanced Salt Solution (HBSS) and thymic slices at a thickness of 400 microns were used for extended culture, whereas 500 micron thick slices were used for two-photon imaging. Thymic slices were transferred to 0.4-micron organotypic cell culture inserts and overlaid with 0.5 to 2 × 10^6 cells in 10 μl of complete DMEM. Cells were applied to slices for 2 hours, washed by gentle, indirect pipetting of phosphate-buffered saline (PBS), and either overlaid with a second cell population or peptide and then glued to a cover glass for two-photon imaging, or were left in culture, as indicated in the figure legends.

Thymocyte labeling

Thymocytes (3 × 10^6 cells/ml) were labeled with 2 μM leakage-resistant Indo-1 (TEFLabs) in complete RPMI for 90 min at 37°C, washed once with 10 ml of RPMI, and were allowed to recover for 60 min in complete RPMI at 37°C. Thymocytes were labeled with 2 μM Seminaphthorhodafluors (SNARF-1) or 0.5 μM Carboxyfluorescein diacetate succinimidyl ester (CFDA-SE) (Invitrogen) at a concentration of 1 × 10^7 cells/ml in PBS for 10 min at 37°C, and then were washed 3 times with complete DMEM before being added to the thymic slices.

Flow cytometry

Thymic slices were dissociated to single cell suspensions with glass tissue grinders and were filtered with nylon mesh. The following antibodies were used for flow cytometric analysis: PerCPefluor710-conjugated anti-CD4, efluor450-conjugated anti-CD8α, allophycocyanin (APC)-conjugated anti-CD8α, anti-CD8β-APC, phycoerythrin (PE)-Cy7–conjugated anti-CD24, anti-CD69–biotin, fluorescein isothiocyanate (FITC)-conjugated anti-Ly5.1, anti-Ly5.2-PE, anti-GzmB–FITC, anti–IFNγ-PE-Cy7, anti-Thy1.2-biotin, anti-CD11c-PE, anti-

MHC I–APC, anti-MHC II–FITC, anti-CD80–FITC, anti-CD86-APC, and anti-CD40-FITC. Streptavidin-APC and streptavidin-PerCP-Cy5.5 were used to detect bound biotinylated antibodies. For intracellular staining, the Cytofix/Cytoperm Fixation/Permeabilization Kit with GolgiPlug (BD biosciences) was used according to the manufacturer's instructions. Data were collected on an LSRII flow cytometer (BD biosciences) and were analyzed with FloJo software (Tree Star).

T cell activation

96-well, non-tissue culture–treated, flat-bottom plates were coated with anti-mouse CD3 (2C11) antibody (5 mg/ml). Thymic slices were dissociated to a single-cell suspension 96 hours after culture initiation and were plated at 1×10^5 cells per well in complete RPMI medium containing anti-mouse CD28 (PV-1) antibody (2 mg/ml). Seventy-two hours later, cells were further stimulated with phorbol-12-myristate-13-acetate (PMA) and ionomycin (Sigma) in the presence of GolgiPlug (BD biosciences).

Preparation of dendritic cells

Bone marrow was harvested from the femurs and tibias of mice and was resuspended in complete RPMI supplemented with recombinant murine granulocyte macrophage colony-stimulating factor (GM-CSF, 10 ng/ml, Peprotech) at 5×10^6 cells per 10ml, and were plated in petri dishes. On day two of culture, another 10 ml of complete RPMI with GM-CSF was added, and every other day, half-media changes were performed. Semi-adherent cells were harvested on day 8 of culture. Thymic DCs were obtained by digestion of thymic tissue with collagenase followed by depletion of thymocytes with an anti-mouse Thy1.2-biotin antibody with the EasySep Biotin Positive Selection Kit (STEMCELL Technologies) according to the manufacturer's instructions.

Peptides

The SIINFEKL peptide and the Q7, T4, and Q4 variants were either purchased from AnaSpec or were synthesized by Invitrogen. Bone marrow–derived DCs were resuspended at 1×10^7 cells/ml and loaded with peptide at a final concentration of 1 nM for 20 min at 37°C. Cells were subsequently washed three times with complete DMEM and added to thymic slices at 1×10^6 cells/10 μl of complete DMEM. Alternatively, 1 nM peptide was added directly to the top of the thymic slice and in the media under the cell culture insert.

Two-photon imaging

All imaging was performed 2 to 4 hours after the addition of thymocytes or peptide to the thymic slices, which were maintained at 37°C in oxygenated, phenol red–free DMEM during imaging. Images were acquired on a custom-built two-photon microscope with a 20×/0.95 Olympus objective and a Spectra-Physics MaiTai Laser tuned to 720 nm (for imaging of Indo-1) or 920 nm (for all other imaging). Ratiometric Ca^{2+} signals were collected with 440 and 510 nm dichroic mirrors and 400/45 and 480/50 bandpass filters. Signals from CFP and CFDA-SE were separated with 495 and 560 nm dichroic mirrors, and signals from YFP and SNARF were separated with 560 and 650 nm dichroic mirrors. Image areas of 172 ×

143 microns to a depth of 200 microns were acquired every 20 s for 20 min with 3-micron z steps starting from beneath the cut surface, using custom software.

Image analysis

Imaris software (Bitplane Scientific Software) was used to process and render the two-photon movies to obtain the 3D coordinates of the cells to analyze migratory behavior as well as the relative intensity of the Indo-1 dye for Ca^{2+} analysis. Two-photon image data were analyzed with standard and custom-written MATLAB scripts (Mathworks), Image J, and Excel. The codes used are available upon request. Graphing and statistical analysis was performed with GraphPad Prism software. For corrected Ca^{2+} values, 0.675 (the average value under non-selecting conditions for OT1tg cells) or 0.585 (the average value under non-selecting conditions for HY^{CD4}tg cells) was subtracted from the raw Ca^{2+} ratio values, and cells were considered to be undergoing signaling when the corrected Ca^{2+} ratio was >0.2 for ≥ 1 time point during the duration of a cell track. Cell tracks were categorized as "lo" (or non-signaling) if the corrected Ca^{2+} ratio did not increase above 0.2 for the duration of the track. Cell tracks were categorized as "lo-hi" (or of intermittent signaling) if the corrected Ca^{2+} value reached a value of ≥ 0.2 at least once over the duration of the track and the average corrected Ca^{2+} ratio was < 0.1. Cell tracks were categorized as "hi" (or having stable signaling) if the corrected Ca^{2+} value reached a value of ≥ 0.2 at least once over the duration of the track and if the average corrected Ca^{2+} ratio was ≥ 0.1.

Statistical analysis

The Student's t test was performed as appropriate and values were considered statistically significant when $P < 0.05$.

Supplementary Material

Refer to Web version on PubMed Central for supplementary material.

Acknowledgments

We thank P. Bousso, B. J. Fowlkes, J. Halkias, B. Weist, K. Taylor, and B. Haley for critical reading of the manuscript. We also thank S.-j. Han and H. Chu for technical assistance and suggestions. **Funding:** This work was supported by the California Institute of Regenerative Medicine post-doctoral training grant TG2-01164 (to H.J.M.) and National Institutes of Health grant AI064227-07 (to E.A.R.).

REFERENCES AND NOTES

1. Starr TK, Jameson SC, Hogquist KA. Positive and negative selection of T cells. Annu Rev Immunol. 2003; 21:139–176. [PubMed: 12414722]
2. Daniels MA, Teixeiro E, Gill J, Hausmann B, Roubaty D, Holmberg K, Werlen G, Hollander GA, Gascoigne NR, Palmer E. Thymic selection threshold defined by compartmentalization of Ras/MAPK signalling. Nature. 2006; 444:724–729. [PubMed: 17086201]
3. Anderson G, Moore NC, Owen JJ, Jenkinson EJ. Cellular interactions in thymocyte development. Annu Rev Immunol. 1996; 14:73–99. [PubMed: 8717508]
4. Ehrlich LI, Oh DY, Weissman IL, Lewis RS. Differential contribution of chemotaxis and substrate restriction to segregation of immature and mature thymocytes. Immunity. 2009; 31:986–998. [PubMed: 19962328]

5. Halkias J, Melichar HJ, Taylor KT, Ross JO, Yen B, Cooper SB, Winoto A, Robey EA. Opposing chemokine gradients control human thymocyte migration in situ. J Clin Invest. 2013; 123:2131–2142. [PubMed: 23585474]
6. Ladi E, Schwickert TA, Chtanova T, Chen Y, Herzmark P, Yin X, Aaron H, Chan SW, Lipp M, Roysam B, Robey EA. Thymocyte-dendritic cell interactions near sources of CCR7 ligands in the thymic cortex. J Immunol. 2008; 181:7014–7023. [PubMed: 18981121]
7. Le Borgne M, Ladi E, Dzhagalov I, Herzmark P, Liao YF, Chakraborty AK, Robey EA. The impact of negative selection on thymocyte migration in the medulla. Nat Immunol. 2009; 10:823–830. [PubMed: 19543275]
8. Witt CM, Raychaudhuri S, Schaefer B, Chakraborty AK, Robey EA. Directed migration of positively selected thymocytes visualized in real time. PLoS Biol. 2005; 3:e160. [PubMed: 15869324]
9. Bhakta NR, Oh DY, Lewis RS. Calcium oscillations regulate thymocyte motility during positive selection in the three-dimensional thymic environment. Nat Immunol. 2005; 6:143–151. [PubMed: 15654342]
10. Hogquist KA. Signal strength in thymic selection and lineage commitment. Curr Opin Immunol. 2001; 13:225–231. [PubMed: 11228417]
11. Germain RN. T-cell development and the CD4-CD8 lineage decision. Nat Rev Immunol. 2002; 2:309–322. [PubMed: 12033737]
12. Baldwin TA, Sandau MM, Jameson SC, Hogquist KA. The timing of TCR alpha expression critically influences T cell development and selection. J Exp Med. 2005; 202:111–121. [PubMed: 15998791]
13. Laufer TM, DeKoning J, Markowitz JS, Lo D, Glimcher LH. Unopposed positive selection and autoreactivity in mice expressing class II MHC only on thymic cortex. Nature. 1996; 383:81–85. [PubMed: 8779719]
14. van Meerwijk JP, Marguerat S, Lees RK, Germain RN, Fowlkes BJ, MacDonald HR. Quantitative impact of thymic clonal deletion on the T cell repertoire. J Exp Med. 1997; 185:377–383. [PubMed: 9053438]
15. Bix M, Raulet D. Inefficient positive selection of T cells directed by haematopoietic cells. Nature. 1992; 359:330–333. [PubMed: 1406938]
16. Dzhagalov IL, Chen KG, Herzmark P, Robey EA. Elimination of self-reactive T cells in the thymus: a timeline for negative selection. PLoS Biol. 2013; 11:e1001566. [PubMed: 23700386]
17. Donnadieu E, Bismuth G, Trautmann A. Antigen recognition by helper T cells elicits a sequence of distinct changes of their shape and intracellular calcium. Curr Biol. 1994; 4:584–595. [PubMed: 7953532]
18. Negulescu PA, Krasieva TB, Khan A, Kerschbaum HH, Cahalan MD. Polarity of T cell shape, motility, and sensitivity to antigen. Immunity. 1996; 4:421–430. [PubMed: 8630728]
19. Wei SH, Safrina O, Yu Y, Garrod KR, Cahalan MD, Parker I. Ca2+ signals in CD4+ T cells during early contacts with antigen-bearing dendritic cells in lymph node. J Immunol. 2007; 179:1586–1594. [PubMed: 17641025]
20. McCaughtry TM, Baldwin TA, Wilken MS, Hogquist KA. Clonal deletion of thymocytes can occur in the cortex with no involvement of the medulla. J Exp Med. 2008; 205:2575–2584. [PubMed: 18936237]
21. Lindquist RL, Shakhar G, Dudziak D, Wardemann H, Eisenreich T, Dustin ML, Nussenzweig MC. Visualizing dendritic cell networks in vivo. Nat Immunol. 2004; 5:1243–1250. [PubMed: 15543150]
22. Aramburu J, Yaffe MB, Lopez-Rodriguez C, Cantley LC, Hogan PG, Rao A. Affinity-driven peptide selection of an NFAT inhibitor more selective than cyclosporin A. Science. 1999; 285:2129–2133. [PubMed: 10497131]
23. Ebert PJ, Ehrlich LI, Davis MM. Low ligand requirement for deletion and lack of synapses in positive selection enforce the gauntlet of thymic T cell maturation. Immunity. 2008; 29:734–745. [PubMed: 18993085]

24. Marangoni F, Murooka TT, Manzo T, Kim EY, Carrizosa E, Elpek NM, Mempel TR. The transcription factor NFAT exhibits signal memory during serial T cell interactions with antigen-presenting cells. Immunity. 2013; 38:237–249. [PubMed: 23313588]
25. Lodygin D, Odoardi F, Schlager C, Korner H, Kitz A, Nosov M, van den Brandt J, Reichardt HM, Haberl M, Flugel A. A combination of fluorescent NFAT and H2B sensors uncovers dynamics of T cell activation in real time during CNS autoimmunity. Nat Med. 2013
26. Borriello F, Sethna MP, Boyd SD, Schweitzer AN, Tivol EA, Jacoby D, Strom TB, Simpson EM, Freeman GJ, Sharpe AH. B7-1 and B7-2 have overlapping, critical roles in immunoglobulin class switching and germinal center formation. Immunity. 1997; 6:303–313. [PubMed: 9075931]
27. Sligh JE Jr, Ballantyne CM, Rich SS, Hawkins HK, Smith CW, Bradley A, Beaudet AL. Inflammatory and immune responses are impaired in mice deficient in intercellular adhesion molecule 1. Proc Natl Acad Sci U S A. 1993; 90:8529–8533. [PubMed: 8104338]
28. Lo WL, Donermeyer DL, Allen PM. A voltage-gated sodium channel is essential for the positive selection of CD4(+) T cells. Nat Immunol. 2012; 13:880–887. [PubMed: 22842345]
29. Azzam HS, Grinberg A, Lui K, Shen H, Shores EW, Love PE. CD5 expression is developmentally regulated by T cell receptor (TCR) signals and TCR avidity. J Exp Med. 1998; 188:2301–2311. [PubMed: 9858516]
30. Merkenschlager M, Graf D, Lovatt M, Bommhardt U, Zamoyska R, Fisher AG. How many thymocytes audition for selection? J Exp Med. 1997; 186:1149–1158. [PubMed: 9314563]
31. Stritesky GL, Jameson SC, Hogquist KA. Selection of self-reactive T cells in the thymus. Annu Rev Immunol. 2012; 30:95–114. [PubMed: 22149933]
32. Moreau HD, Lemaitre F, Terriac E, Azar G, Piel M, Lennon-Dumenil AM, Bousso P. Dynamic in situ cytometry uncovers T cell receptor signaling during immunological synapses and kinapses in vivo. Immunity. 2012; 37:351–363. [PubMed: 22683126]
33. Pace L, Tempez A, Arnold-Schrauf C, Lemaitre F, Bousso P, Fetler L, Sparwasser T, Amigorena S. Regulatory T cells increase the avidity of primary CD8+ T cell responses and promote memory. Science. 2012; 338:532–536. [PubMed: 23112334]
34. Skokos D, Shakhar G, Varma R, Waite JC, Cameron TO, Lindquist RL, Schwickert T, Nussenzweig MC, Dustin ML. Peptide-MHC potency governs dynamic interactions between T cells and dendritic cells in lymph nodes. Nat Immunol. 2007; 8:835–844. [PubMed: 17632517]
35. Stritesky GL, Xing Y, Erickson JR, Kalekar LA, Wang X, Mueller DL, Jameson SC, Hogquist KA. Murine thymic selection quantified using a unique method to capture deleted T cells. Proc Natl Acad Sci U S A. 2013; 110:4679–4684. [PubMed: 23487759]
36. Daley SR, Hu DY, Goodnow CC. Helios marks strongly autoreactive CD4+ T cells in two major waves of thymic deletion distinguished by induction of PD-1 or NF-kappaB. J Exp Med. 2013; 210:269–285. [PubMed: 23337809]
37. Murata S, Sasaki K, Kishimoto T, Niwa S, Hayashi H, Takahama Y, Tanaka K. Regulation of CD8+ T cell development by thymus-specific proteasomes. Science. 2007; 316:1349–1353. [PubMed: 17540904]
38. Honey K, Nakagawa T, Peters C, Rudensky A. Cathepsin L regulates CD4+ T cell selection independently of its effect on invariant chain: a role in the generation of positively selecting peptide ligands. J Exp Med. 2002; 195:1349–1358. [PubMed: 12021314]
39. Nakagawa T, Roth W, Wong P, Nelson A, Farr A, Deussing J, Villadangos JA, Ploegh H, Peters C, Rudensky AY. Cathepsin L: critical role in Ii degradation and CD4 T cell selection in the thymus. Science. 1998; 280:450–453. [PubMed: 9545226]
40. Degermann S, Surh CD, Glimcher LH, Sprent J, Lo D. B7 expression on thymic medullary epithelium correlates with epithelium-mediated deletion of V beta 5+ thymocytes. J Immunol. 1994; 152:3254–3263. [PubMed: 7511640]
41. Hadjantonakis AK, Macmaster S, Nagy A. Embryonic stem cells and mice expressing different GFP variants for multiple non-invasive reporter usage within a single animal. BMC Biotechnol. 2002; 2:11. [PubMed: 12079497]
42. Grusby MJ, Auchincloss H Jr, Lee R, Johnson RS, Spencer JP, Zijlstra M, Jaenisch R, Papaioannou VE, Glimcher LH. Mice lacking major histocompatibility complex class I and class II molecules. Proc Natl Acad Sci U S A. 1993; 90:3913–3917. [PubMed: 8483910]

43. Hogquist KA, Jameson SC, Heath WR, Howard JL, Bevan MJ, Carbone FR. T cell receptor antagonist peptides induce positive selection. Cell. 1994; 76:17–27. [PubMed: 8287475]

44. Schaefer BC, Schaefer ML, Kappler JW, Marrack P, Kedl RM. Observation of antigen-dependent CD8+ T-cell/dendritic cell interactions in vivo. Cell Immunol. 2001; 214:110–122. [PubMed: 12088410]

45. Dzhagalov IL, Melichar HJ, Ross JO, Herzmark P, Robey EA. Two-photon imaging of the immune system. Curr Protoc Cytom. 2012; Chapter 12(Unit12):26. [PubMed: 22470153]

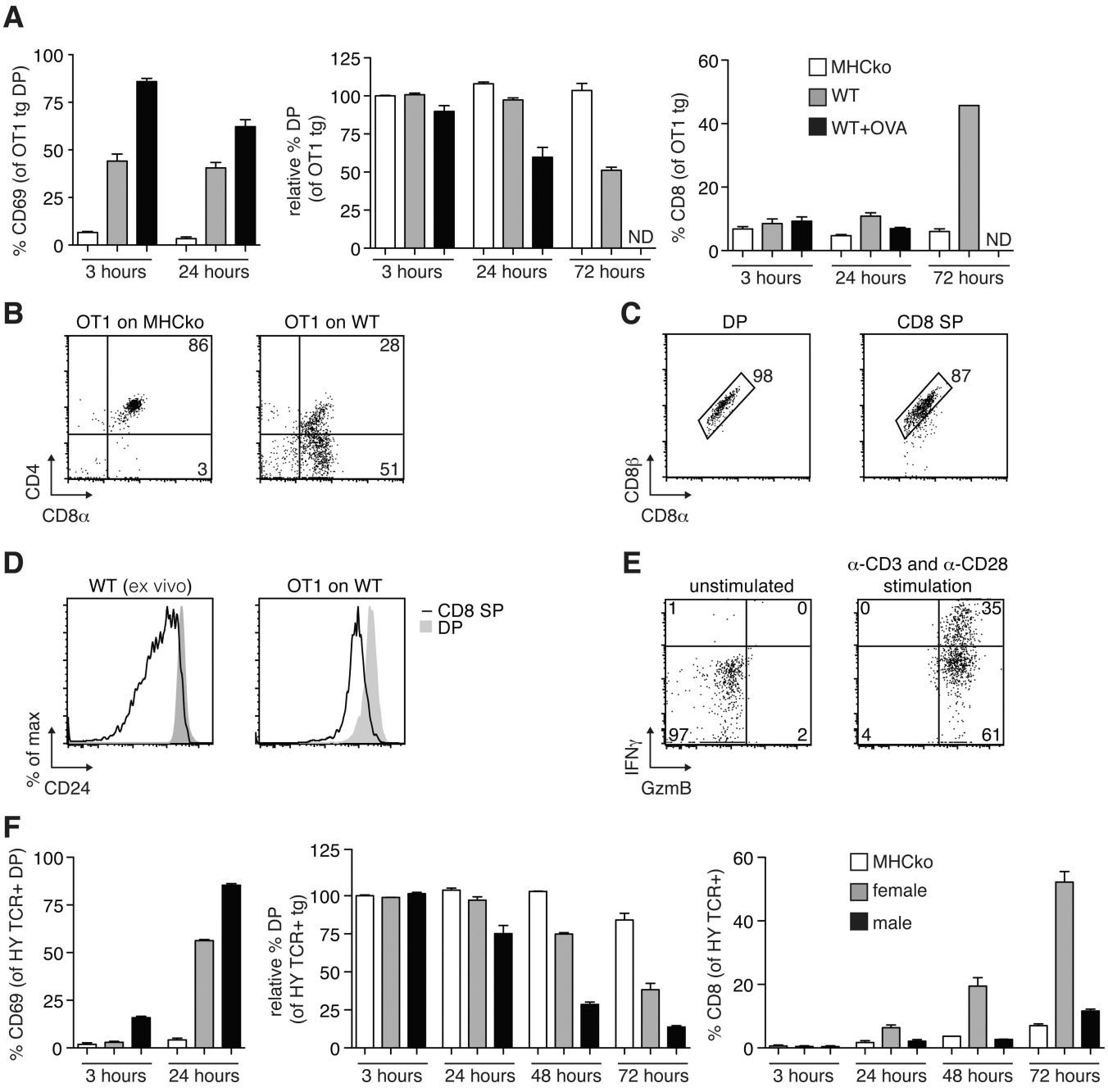

Fig. 1. Analysis of positive and negative selection of thymocytes on thymic slices

(**A**) Thymic slices prepared from MHC-deficient mice (MHCko) or wild-type (WT) mice (which were left untreated or were treated with OVA peptide) were overlaid with OT1tg DP cells. Two hours later, the slices were washed, and thymocytes were harvested at the indicated times for flow cytometric analysis. Left: Percentages of OT1tg DP thymocytes that were positive for CD69 at the indicated times. Middle: Percentages of OT1tg DP thymocytes that were present at the indicated times relative to the numbers of starting OT1tg cells. Right: Percentages of OT1tg $CD8^+$ SP cells at the indicated times. Data are means ± SEM from at least three thymic slices from two or more independent experiments. ND, not

detected. (**B**) OT1tg cells harvested from MHCko or WT thymic slices after 72 hours of incubation were analyzed by flow cytometry with antibodies against CD4 and CD8α. Representative data from triplicate thymic slices from more than three independent experiments. (**C**) The cell-surface abundance of the CD8αβ heterodimer on OT1tg DP or $CD8^+$ SP thymocytes after 72 hours of incubation on WT thymic slices was assessed by flow cytometric analysis with antibodies against CD8α and CD8β. Representative data from triplicate thymic slices from two independent experiments. (**D**) Representative histograms from the flow cytometric analysis of CD24 on ex vivo WT thymocytes (left) or OT1tg thymocytes after 96 hours of incubation on WT thymic slices (right). Representative data from triplicate thymic slices from two independent experiments. (**E**) Flow cytometric analysis of the relative abundances of granzyme B (GzmB) and IFN-γ in OT1tg $CD8^+$ SP thymocytes that were harvested after 96 hours of incubation on WT thymic slices that then were subsequently activated in vitro with plate-bound anti-CD3 and soluble anti-CD28 antibodies. Representative data from triplicate thymic slices from two independent experiments. (**F**) Left: Percentages of $T3.70^+$ HY TCR tg DP cells that were positive for CD69 at the indicated times. Middle: Percentages of DP thymocytes that were present at the indicated times relative to the proportions of starting $T3.70^+$ HY TCR tg DP cells. Right: Percentages of $CD8^+$ SP cells at the indicated times. Data are means ± SEM of triplicate slices from one experiment and are representative of at least experiments.

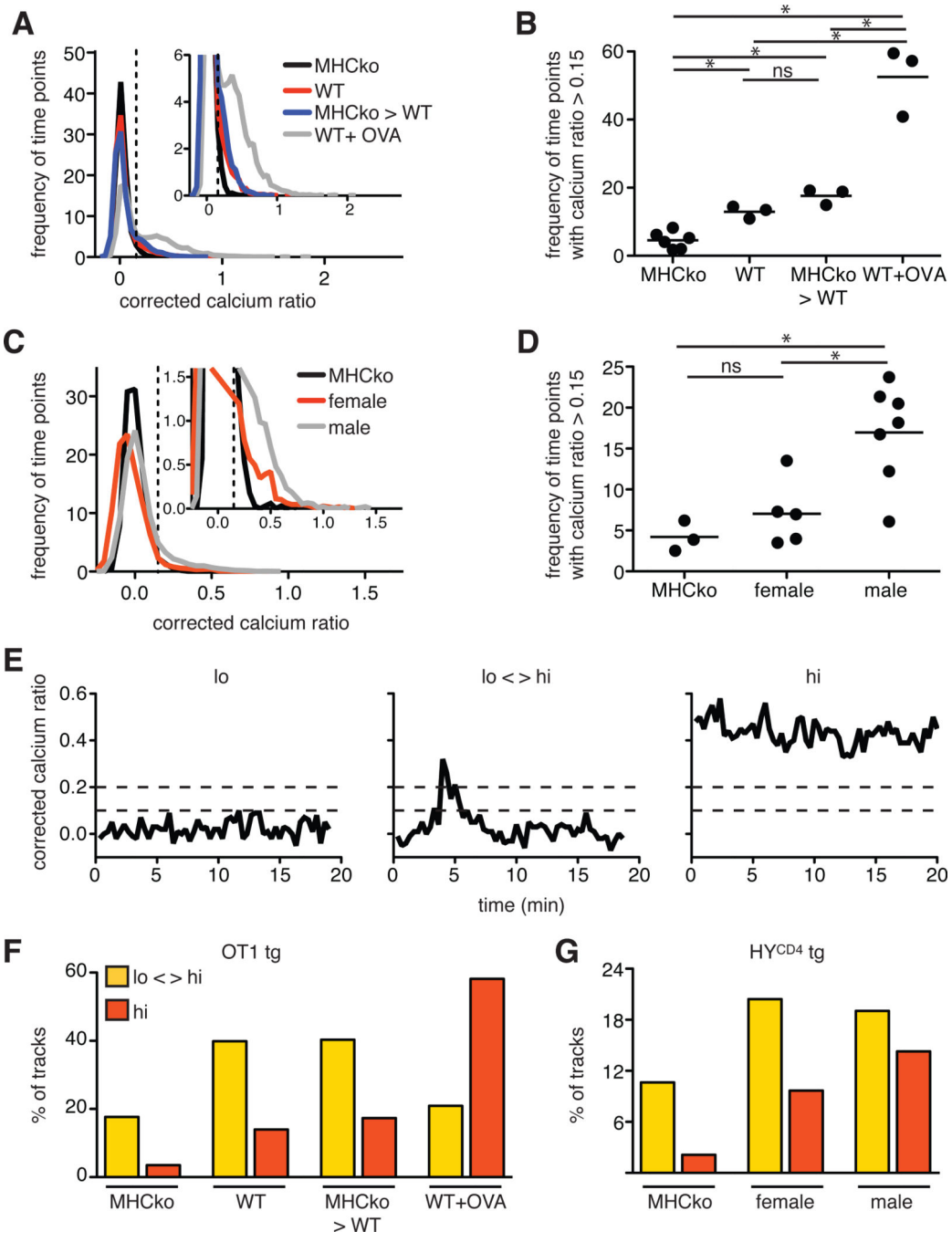

Fig. 2. Thymocytes undergoing positive or negative selection in situ exhibit distinct Ca^{2+} signals

(**A**) Plot of the frequency of time points against the corrected Ca^{2+} ratio of Indo-1–labeled OT1tg thymocytes incubated on thymic slices presenting positive-selecting (WT and MHCko→WT) or negative-selecting (WT+OVA) peptides. The dashed vertical line indicates the ratio above which increased cytosolic Ca^{2+} concentrations occurred. Inset: An enlarged portion of the graph. Unless otherwise noted throughout the manuscript, for imaging quantification, data are compiled from a minimum of three movies from two independent experiments for each condition. For the MHCko thymic slice: n = 5416 time

points (195 cell tracks); WT: n = 7210 time points (195 tracks); MHCko→WT: n = 5896 time points (159 tracks); and WT+OVA: n = 7979 time points (197 tracks). (**B**) Frequency of time points that had a corrected Ca^{2+} ratio >0.15 for OT1tg cells. Each dot represents a single movie. (**C**) The frequency of time points plotted against the corrected Ca^{2+} ratios of Indo-1–loaded HY^{CD4}tg thymocytes on thymic slices presenting positive-selecting (female) or negative-selecting (male) peptides. Inset: An enlarged portion of the graph. (**D**) Frequency of time points that had a corrected Ca^{2+} ratio >0.15 for HY^{CD4}tg cells. Each dot represents a single movie. (**E**) Examples of the corrected Ca^{2+} ratios of individual cells categorized as having “lo” (non-signaling) tracks, “lo-hi” (intermittent signaling) tracks, or “hi” (stable signaling) tracks. Corrected Ca^{2+} ratios of 0.1 and 0.2 are indicated by dashed horizontal lines. (**F**) Percentages of the tracks of OT1tg cells (where track lengths were >20 time points) in the indicated Ca^{2+} signaling categories on non-selecting MHCko slices, positively selecting WT or MHCko→WT slices, or negatively selecting WT slices with OVAp. For MHCko: n = 113 tracks; WT: n = 143 tracks; MHCko→WT: n = 119 tracks; and WT+OVA: n = 153 tracks. (**G**) Percentages of the tracks of HY^{CD4}tg cells (where track lengths were >20 time points) in the indicated Ca^{2+} signaling categories on non-selecting MHCko slices, positively selecting WT female slices, or positive and negatively selecting WT male slices. For MHCko: n = 72 tracks; WT female: n = 93 tracks; and WT male: n = 42 tracks.

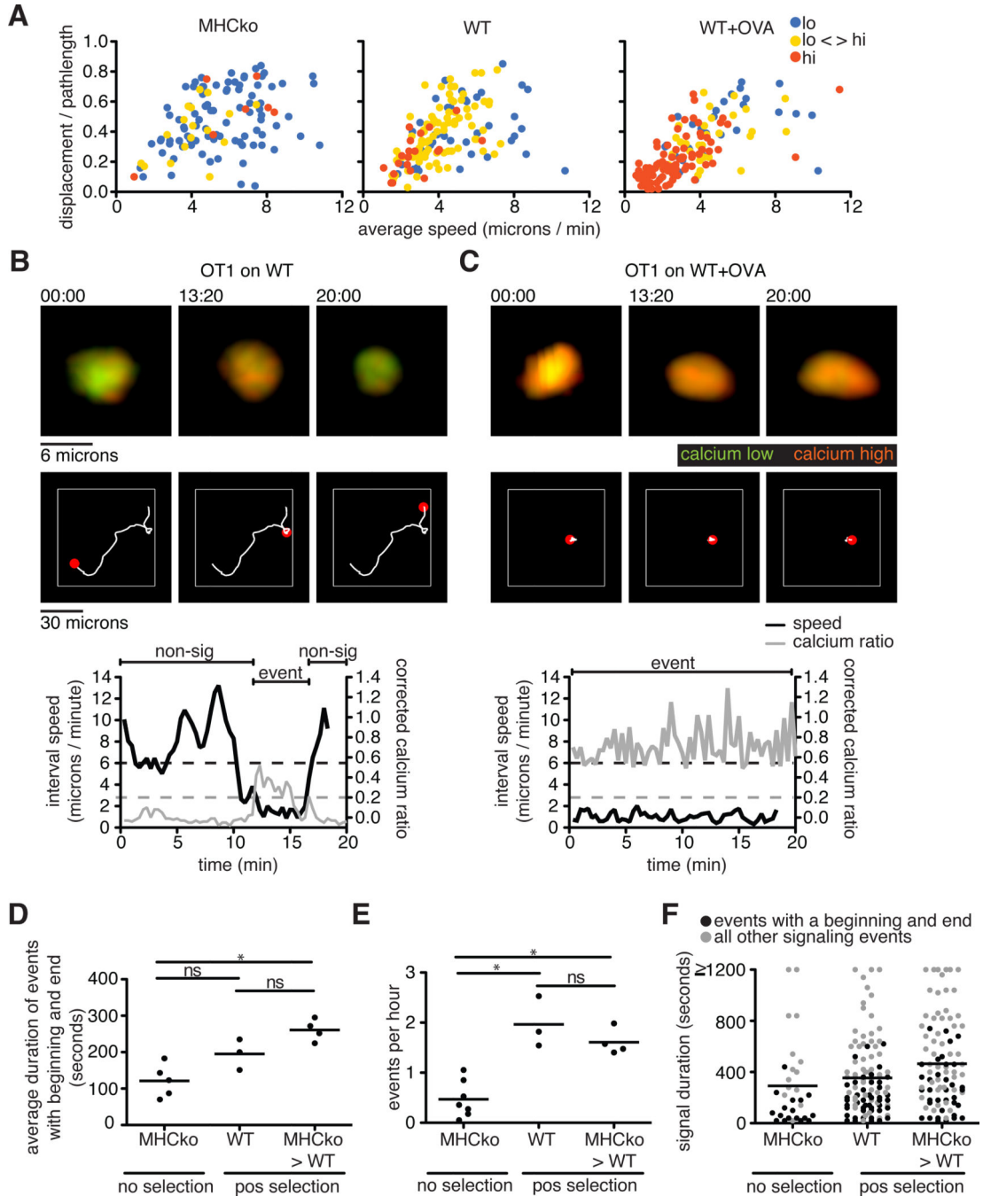

Fig. 3. Thymocytes exhibit an inverse correlation between the extent of their Ca^{2+} signaling and their motility

(**A**) Analysis of the average speed and the straightness (displacement / pathlength) of OT1tg cells under non-selecting, positive-selecting, and negative-selecting conditions. Each dot indicates an individual cell track (where track lengths were >20 time points) and is color-coded according to its Ca^{2+} signaling category. For MHCko: n = 113 tracks; WT: n = 143 tracks; WT+OVA: n = 153 tracks. (**B** and **C**) Representative images, Ca^{2+} signaling, and motility plots of an OT1tg cell signaling on (B) a positively selecting WT slice or (C) a WT

slice in the presence of OVA (negative selection). Top: Green indicates unbound Indo-1 dye, whereas red indicates Ca^{2+}-bound dye over time. Middle: The white line indicates the cell track for the duration of the movie with the red spot indicating the location of the cell at the time points indicated above the top panels. Bottom: Corrected Ca^{2+} ratios in gray and speed in black. The dashed gray line indicates a Ca^{2+} signaling threshold of 0.2, whereas the dashed black line indicates a speed threshold of 6 microns/min based on the average speed of the cell over five time points (100 s). Regions of the cell track that were identified as containing signaling events (event) and non-signaling events (non-sig) are indicated above the traces. (**D**) Quantification of the duration of those Ca^{2+} signaling events that both began and ended within the imaging period under non-selecting and positive-selecting conditions. Each dot represents an average value from a single movie. (**E**) Quantification of the frequency of Ca^{2+} signaling events under non-selecting and positive-selecting conditions (that is, the number of signaling events that began per hour). Each dot represents an average value from a single movie. (**F**) Each dot represents the duration of individual signaling events in non-selecting and positive-selecting conditions. Black dots indicate signaling events that had a beginning and an end during the imaging period, whereas gray dots indicate all other signaling events. Lines indicate the averages of all signaling events. For MHCko: n = 31 tracks; WT: n = 102 tracks; MHCko→WT: n = 93 tracks.

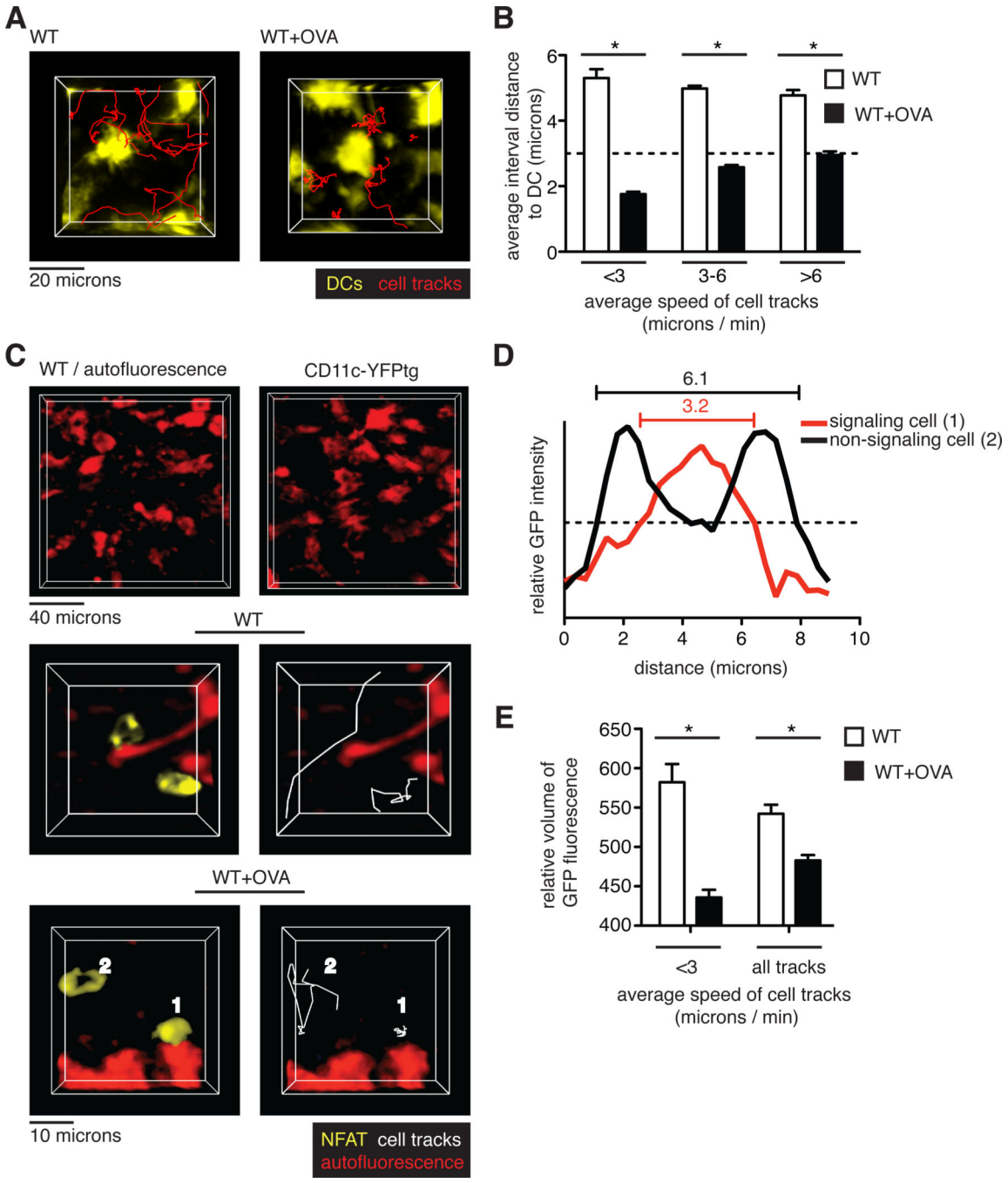

Fig. 4. TCR signaling predominantly occurs near DCs during negative selection

(**A**) Representative images of cell tracks of OT1tg DP cells (red) in the cortex of the indicated thymic slices containing CD11c-YFP–labeled DCs. (**B**) Analysis of the interactions between thymocytes and DCs. Quantification of the average distances between pre-selection OT1tg DP cells and CD11c-YFPtg DCs versus average track speed in the absence or presence of the negatively selecting OVA peptide. The dashed line indicates cell contact (that is, when the distance between cells was approximately the radius of a typical DP cell.) Data are quantified from one movie and are representative of three movies. WT: n

= 103 tracks; WT+OVA: n = 65 tracks. (**C** to **E**) OT1 tg DP thymocytes expressing NFAT-GFP were overlaid on WT thymic slices or WT thymic slices treated with OVA peptide. (C) Top: Representative images of autofluorescent cells in WT thymic slices (left) as compared to DCs visualized in a CD11c-YFPtg thymic slice (right). Middle and bottom: Representative images of NFAT-GFP–expressing, pre-selection OT1tg DP thymocytes relative to autofluorescent signals in WT slices (middle) and WT+OVA slices (bottom). Examples of NFAT-GFP in the nucleus of a non-migrating thymocyte (labeled as 1) and in the cytoplasm of a migrating thymocyte (labeled as 2) are indicated in negatively selecting WT+OVA conditions. (D) Distribution of fluorescence throughout the length of the labeled cells depicted in (C) The dashed, horizontal line indicates the fluorescence threshold used to determine the cell volume. (E) Analysis of the relative volume of NFAT-GFP fluorescence versus average track speed in OT1tg DP thymocytes on WT slices in the presence or absence of OVA peptide. Data are quantified from one movie and are representative of three movies. WT: n = 15 tracks; WT+OVA: n = 31 tracks.

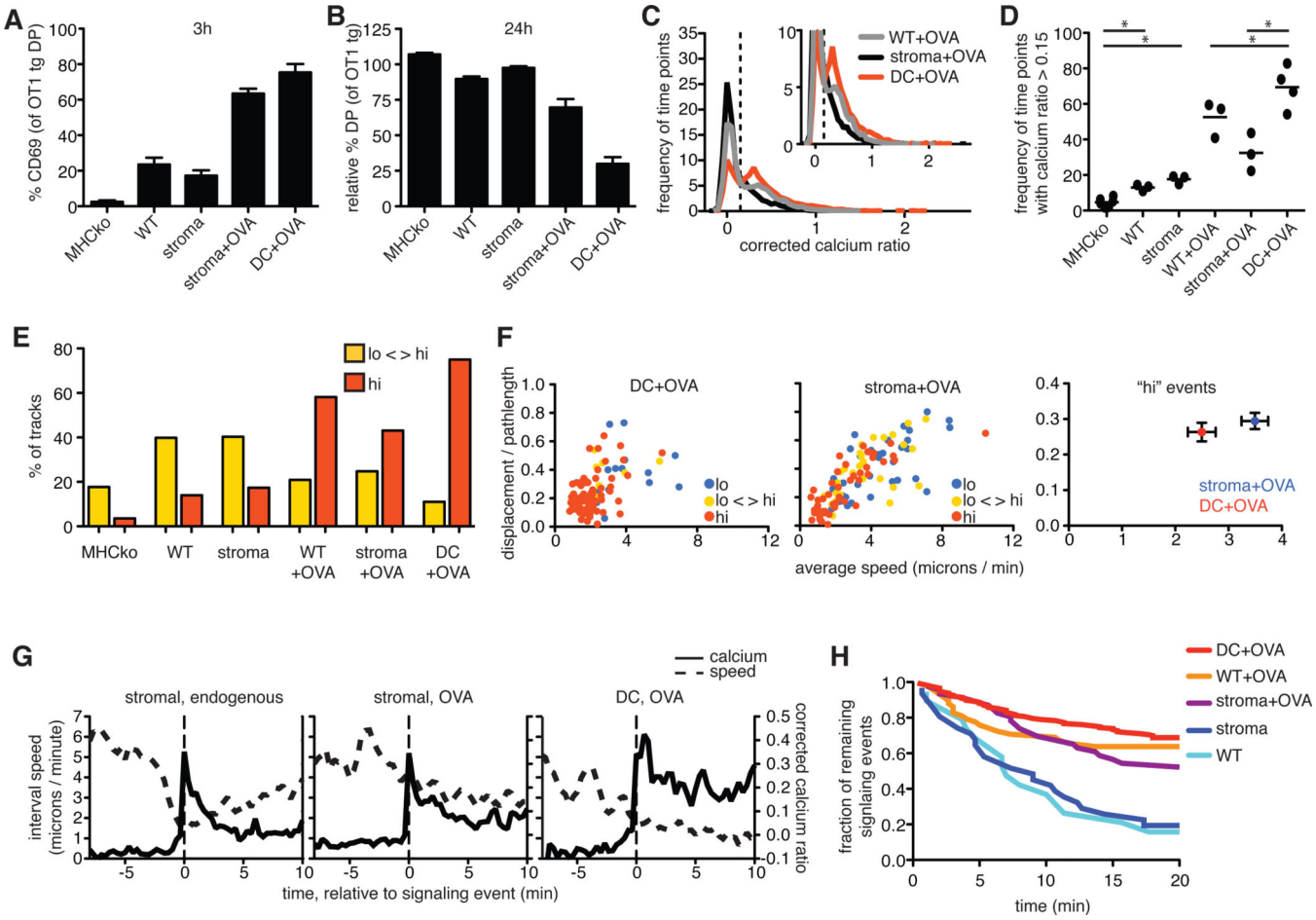

Fig. 5. Radiation-resistant stromal cells do not support effective negative selection or sustained Ca^{2+} signaling

OT1tg cells were overlaid on the indicated thymic slices in the absence or presence of OVA peptide presented either by DCs or by radiation-resistant cells from MHCko→WT bone marrow chimeras (stroma). (**A**) Percentages of DP thymocytes that expressed cell-surface CD69 3 hours after the addition of OVA peptide. (**B**) Analysis of the relative decrease in the percentages of OT1tg DP thymocytes 24 hours after the addition of OVA peptide. Data in (A) and (B) are means ± SEM of triplicate slices from one experiment and are representative of at least two experiments. (**C**) Plot of the frequency of time points against corrected Ca^{2+} ratios of Indo-1–labeled OT1tg thymocytes incubated on thymic slices in the presence or absence of OVA peptide. The dashed vertical line indicates the ratio above which increased cytosolic Ca^{2+} concentrations occurred. Inset: An enlarged portion of the graph. Data for WT+OVA from Fig. 2A are included for comparison. Stroma+OVA: n = 5348 time points (153 tracks); DC+OVA: n = 5444 time points (114 tracks). (**D**) Frequency of time points that had corrected Ca^{2+} values >0.15 for OT1tg cells overlaid on the indicated thymic slices. Each dot represents a single movie. Data in the first four conditions are from Fig. 2B and are included for reference. (**E**) Percentages of the tracks of OT1tg cells (where track lengths were >20tps) on the indicated thymic slices in the indicated Ca^{2+} signaling categories. The MHCko, WT, MHCko→WT, and WT+OVA conditions are included from Fig. 2F for the

purpose of comparison. Stroma+OVA: n = 5348 time points (153 tracks); DC+OVA: n = 5444 time points (114 tracks). (**F**) Analysis of the speed and straightness (displacement / pathlength) of OT1tg cells encountering OVA peptide presented by DCs or stromal cells. Left and middle: Each dot indicates an individual cell track and is color-coded according to the Ca^{2+} signaling category. DC+OVA: n = 98 tracks; Stroma+OVA: n = 109 tracks. Right: Average values ± SEM of the "hi" signaling tracks. (**G**) Average corrected Ca^{2+} ratios and interval speeds of signaling tracks aligned at time = 0 as the signal-triggering event (indicated by the dashed vertical lines) over time of OT1tg cells overlaid on slices. Stromal, endogenous: n = 37 tracks; Stromal, OVA: n = 30 tracks; DC, OVA: n = 14 tracks. (**H**) Fraction of those thymocytes that were signaling at the beginning of each imaging run that remained signaling over time. Numbers of signaling cells at time = 0: DC+OVA: n = 176; WT+OVA: n = 58; stroma+OVA: n = 46; stroma: n = 31; WT: n = 19.

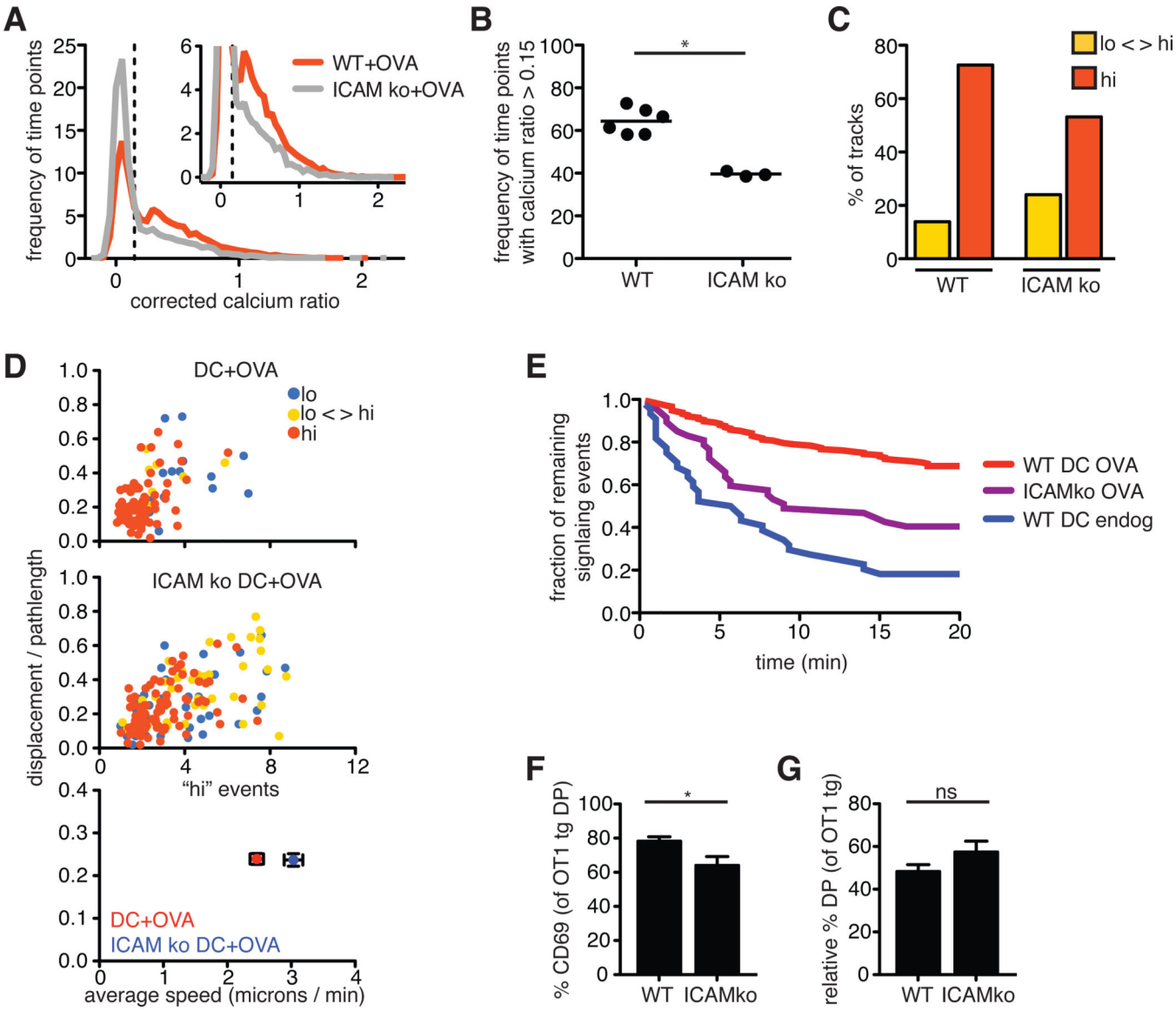

Fig. 6. Adhesion molecules contribute to sustained Ca^{2+} signaling during negative selection

(**A**) Plot of the frequency of time points against the corrected Ca^{2+} ratios of Indo-1–labeled OT1tg thymocytes incubated on thymic slices in the presence of OVA peptide presented by WT or ICAMko DCs. The dashed vertical line indicates the ratio above which increased cytosolic Ca^{2+} concentrations occurred. Inset: An enlarged portion of the graph. WT DCs: n = 15719 time points (332 tracks); ICAMko DCs: n = 8286 time points (176 tracks). (**B**) Frequency of the time points that had corrected Ca^{2+} values >0.15 for OT1tg cells overlaid on MHCko slices in the presence of WT or ICAMko DCs loaded with OVA peptide. Each dot represents one movie from a minimum of two independent experiments. (**C**) Percentages of the tracks of OT1tg cells (where track lengths were >20tps) in the indicated Ca^{2+} signaling categories in the presence of OVA peptide presented by WT or ICAMko DCs. WT +OVA: n = 290 tracks; ICAM ko: n = 159 tracks. (**D**) Top and middle: Plots of the speed and straightness (displacement / pathlength) of the tracks of OT1tg cells (where track

lengths were >20tps) that encountered OVA peptide presented by WT or ICAMko DCs. Each dot indicates an individual cell track and is color-coded according to the indicated Ca^{2+} signaling categories. WT+OVA: n = 159 tracks; ICAM ko: n = 159 tracks. Bottom: Average values ± SEM of the "hi" signaling tracks. (**E**) Persistence of signaling over time in the absence or presence of OVA peptide presented by WT or ICAMko DCs. Data from WT DCs loaded with OVA peptide from Fig. 5G are included for comparison. Numbers of signaling cells at time = 0: ICAMko DC, OVA: n = 47; WT DC, endog: n = 44. (**F**) Analysis of the percentages of DP thymocytes that expressed cell-surface CD69 3 hours after the addition of WT or ICAMko DCs loaded with OVA peptide. (**G**) Relative percentage decreases in the numbers of OT1tg DP cells 24 hours after the addition of WT or ICAMko DCs loaded with OVA peptide. Data are means ± SEM from triplicate slices and are representative of two experiments FOR (F) AND (G).

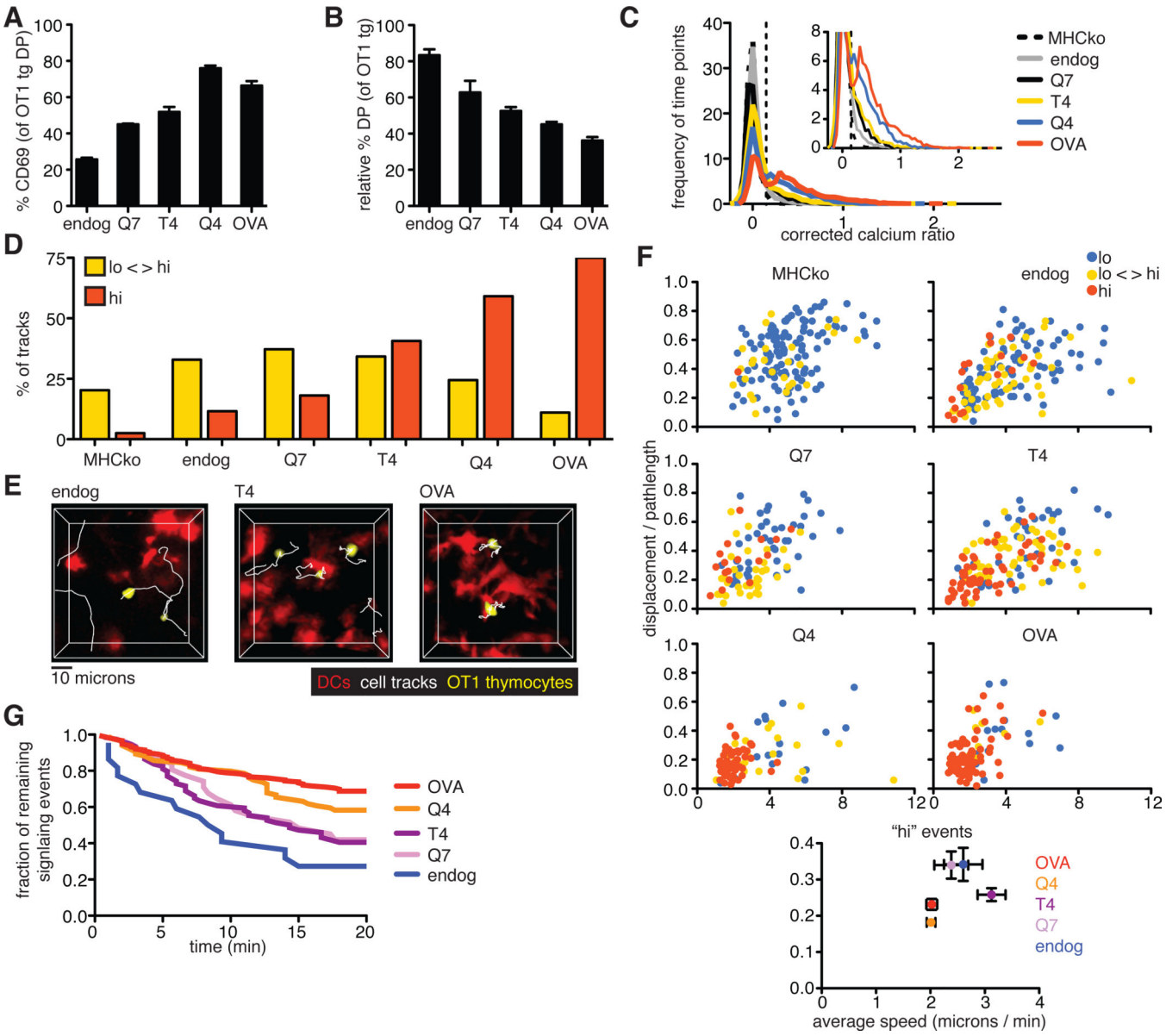

Fig. 7. Increasing ligand potency correlates with a switch from intermittent to sustained Ca^{2+} signaling

(**A**) Analysis of the percentages of DP thymocytes that expressed cell-surface CD69 3 hours after the addition of peptide-loaded DCs. (**B**) Analysis of the relative percentages of OT1tg DP cells 24 hours after the addition of peptide-loaded DCs. Data in (A) and (B) are means ± SEM of triplicate slices from one experiment and are representative of at least two experiments. (**C**) Plot of the frequency of time points against the corrected Ca^{2+} ratios of Indo-1–labeled OT1tg thymocytes incubated on thymic slices in the absence or presence of DCs loaded with APLs. The dashed vertical line indicates the ratio above which increased cytosolic Ca^{2+} concentrations occurred. Inset: An enlarged portion of the graph. Data from DC+OVA slices from Fig. 5C are included for reference. MHCko: n = 7704 time points (131 tracks); Endog: n = 7671 time points (229 tracks); Q7: n = 4565 time points (104 tracks); T4: n = 7714 time points (214 tracks); Q4: n = 5367 time points (110 tracks). (**D**)

Percentages of the tracks of OT1tg cells (where track lengths were >20tps) in the indicated Ca^{2+} signaling categories in the presence of OVA peptide or APLs presented by WT DCs. Data from WT+OVA from Fig. 5E are included for reference. MHCko: n = 149 tracks; Endog: n = 155 tracks; Q7: n = 94 tracks; T4: n = 155 tracks; Q4: n = 98 tracks. (**E**) Representative tracks (white) of OT1tg thymocytes (yellow) interacting with DCs (red) presenting endogenous peptides, T4 peptide, or OVA peptide. (**F**) Plots of the speed and straightness (displacement / pathlength) of the tracks of OT1tg cells (where track lengths were >20tps) in the absence or presence of DCs loaded with the indicated APLs. Each dot indicates an individual cell track and is color-coded according to Ca^{2+} signaling category. WT+OVA data from Fig. 5F are included for reference. MHCko: n = 149 tracks; Endog: n = 155 tracks; Q7: n = 94 tracks; T4: n = 155 tracks; Q4: n = 98 tracks. Bottom: Average values ± SEM of the “hi” signaling tracks. (**G**) Analysis of the persistence of signaling over time in the presence of OVA peptide or APLs presented by WT DCs. OVA data from Fig. 5G and endog data from Fig. 6E are included for comparison. Numbers of signaling cells at time = 0: Q4: n = 84; T4: n = 74; Q7: n = 31.